Transport in Porous Media **6**: 337–358, 1991.

Dispersion of Inert Solutes in Spatially Periodic, Two-Dimensional Model Porous Media

D. A. EDWARDS, M. SHAPIRO, H. BRENNER*, and M. SHAPIRA
Faculty of Mechanical Engineering, Technion–Israel Institute of Technology, Haifa 32000, Israel

(Received: 17 October 1989; revised: 15 August 1990)

Abstract. Taylor dispersion of a passive solute within a fluid flowing through a porous medium is characterized by an effective or Darcy scale, transversely isotropic dispersitivity $\bar{\mathbf{D}}^*$, which depends upon the geometrical microstructure, mean fluid velocity, and physicochemical properties of the system. The longitudinal, $\bar{D}^*_{\parallel}$ and lateral, $\bar{D}^*_{\perp}$ dispersivity components for two-dimensional, spatially periodic arrays of circular cylinders are here calculated by finite element techniques. The effects of bed voidage, packing arrangement, and microscale Péclet and Reynolds numbers upon these dispersivities are systematically investigated.

The longitudinal dispersivity component is found to increase with the microscale Péclet number at a rate less than Pe^2. This accords with previous calculations by Eidsath *et al.* (1983), although the latter calculations were found to yield significantly lower longitudinal dispersivities than those obtained with the present numerical scheme. With increasing Péclet number, a Pe^2 dependence is, however, approached asymptotically, particularly for square cylindrical arrays – owing to the creation of a linear streamline zone between cylinders.

Increasing tortuosity of the intercellular flow pattern reduces the longitudinal dispersivity component and enhances the lateral component. Longitudinal dispersivities for square and hexagonal arrays are found to be quite similar at high porosities; yet they diverge dramatically from one another with decreasing porosity. The longitudinal dispersivity is found to increase markedly with increasing Reynolds number. Comparison of this longitudinal dispersivity with available experimental results shows that $\bar{D}^*_{\parallel}$ experimentally measured for three-dimensional arrays of spheres may be correlated by the present two-dimensional model by an appropriate choice of the array's packing arrangement. In general, the calculated dispersivities were found to be sensitive to the bed packing arrangement and apparently no rationale exists for choosing any one particular geometric microstructure over another for a comparison with existing experimental data. It is thus concluded that existing experimental data pertaining to three-dimensional beds of spherical particles cannot rationally provide a basis for verification of two-dimensional, circular cylindrical dispersion models.

The finite-element scheme employed in this work was tested in the purely diffusive, nonflow limit by calculating the composite diffusivities of square cylindrical arrays for different volume fractions and various dispersed solid-continuous phase diffusivity ratios, subsequently comparing these with existing analytical results. An additional test was provided by comparing calculated with analytical axial dispersivities for transport of a dissolved solute in a Poiseuille flow between two parallel plates.

Key words. Convective dispersion, arrays of cylinders, finite-element solution, coarse-scale transport coefficients, solute diffusivity.

*Department of Chemical Engineering, Massachusetts Institute of Technology, Cambridge, MA 02139, U.S.A.

0. Notation

a	cylinder radius,
$\mathbf{B}(\mathbf{r})$, $\hat{\mathbf{B}}(\mathbf{r})$	intracellular vector fields,
D	molecular diffusivity of solute,
$\bar{D}$	effective molecular diffusivity,
D_d, D_c	respective dispersed- and continuous-phase diffusivities,
$\bar{D}^*_{\parallel}$, $\bar{D}^*_{\perp}$	longitudinal and lateral dispersivity components,
$\bar{\mathbf{D}}^*$	solute dispersivity dyadic,
$\mathbf{f}(\mathbf{r})$	intracellular vector field of Eidsath *et al.* (1983),
h	half distance between two parallel plates,
$\mathbf{i}_1$, $\mathbf{i}_2$	unit basic vectors,
l_1, l_2	linear dimensions of the rectangular unit cell,
$\mathbf{l}_1$, $\mathbf{l}_2$	basic lattice vectors,
n_1, n_2	integers,
$\mathrm{Pe} = 2a\bar{V}/D$	characteristic Péclet number,
$\mathrm{Pe}_p = \frac{2a\bar{V}}{D}\frac{\varepsilon}{1-\varepsilon}$	Péclet number used by Eidsath *et al.* (1983),
$\mathbf{r}$	local intracell position vector,
$\mathbf{R}$	position vector,
$\mathbf{R}_n$	global cell position vector,
$\mathrm{Re} = 2a\rho\bar{V}/\mu$	Reynolds number,
S_p	bed-particle surface(s),
t	time,
$\bar{\mathbf{U}}^*$	solute mean velocity vector,
$\mathbf{v} \equiv \mathbf{v}(\mathbf{r})$	interstitial solute velocity vector field,
$\bar{\mathbf{V}}$	mean interstitial solvent velocity vector,
V_β	'averaging volume'.

Greek Letters

$\alpha = D_d/D_c$	diffusivity ratio,
$\varepsilon = \tau_f/\tau_0$	bed porosity,
τ_f	volume of the intracellular fluid domain,
τ_0	superficial volume of a primitive unit cell,
ν	unit normal vector on S_p.

Operators

$\nabla \equiv \partial/\partial\mathbf{r}$	intracellular gradient operator,
$[\![\ ]\!]$	unit cell jump operator.

Subscripts

$\parallel$	longitudinal component (parallel to the mean flow),
$\perp$	lateral component (perpendicular to the mean flow),
f	fluid,
p	particle.

Superscript

*	global property,
(overbar)	average value.

1. Introduction

The volume occupied by a given mass of dissolved solute injected into a fluid flowing through a porous medium will irreversibly expand as the fluid flows downstream owing to the tortuous geometry of the porous material, variations in local fluid velocity, and molecular diffusion. External forces, chemical reactions and fluid property variations, if present, may also contribute to this spreading process. This phenomenon is known as hydrodynamic dispersion, and has been observed at least since Slichter (1905). Examples of dispersion phenomena (Bear, 1969, 1972) arise when salt and fresh waters meet in coastal aquifers, waste material contaminates a liquid stream, water displaces underground oil during secondary oil recovery processes, salt is leached from soil, and reacting solutes traverse packed-bed chemical reactors.

A simple theoretical explanation of hydrodynamic dispersion is offered by modelling a porous medium as composed of a bundle of identical, parallel, circular cylindrical tubes, through which dissolved solute disperses within a flowing carrier fluid, owing to a combination of molecular diffusion and local velocity inhomogeneity of the Poiseuille flow. Taylor (1953, 1954) and Aris (1956) provided analyses of the resulting 'convective-diffusive' dispersion, demonstrating that the local convective and diffusive motions may be quantified at the global Darcy scale by a dispersivity, $\bar{\mathbf{D}}^*$. For a real porous medium, this dispersivity is a transversely isotropic dyadic with respect to the direction of mean flow and, hence, characterized by two independent nonzero components: a lateral (radial or transverse) dispersivity $\bar{D}^*_\perp$ and a longitudinal (axial) dispersivity $\bar{D}^*_\parallel$. For the tube bundle model the lateral dispersivity is zero, whereas the longitudinal dispersivity is given by the expression

$$\bar{D}^*_\parallel = D + \frac{R^2 \bar{V}^2}{48D}, \tag{1}$$

with D the solute's molecular diffusion coefficient, R the tube radius, and $\bar{V}$ the average solvent velocity.

Real porous media may possess a fairly complicated microstructure, which can scarcely be captured by the 'bundle of tubes' model. To account for the microscale

complexity, Hoagland and Proud'homme (1985) considered solute dispersion in a porous medium characterized by a constricted capillary tube possessing a periodically varying circular cross-section. They numerically calculated the longitudinal dispersivity, the laterial component still being zero. The absence of lateral dispersion is certainly expected, as this 'bundle of constricted tubes' model does not provide a completely faithful description of the geometrical features occurring in real, unconsolidated porous media – namely the existence of transverse interconnections between adjacent longitudinal pores. On the other hand, periodically constricted tube models were successfully applied to deep-bed (Payatakes *et al.*, 1973) and aerosol (Tardos and Gutfinger, 1979) filtration processes. Alternatives to these overly simplistic geometric models often involve probabilistic elements, such as the stochastic models of Aris and Amundson (1957), Saffman (1959, 1960), Simpson (1969) and Koch and Brady (1985), random diameter capillary tube models (Simon and Kelsey, 1971, 1972), or the volume-averaging models of Bear (1972) and Carbonell and Whitaker (1983). Reviews of these statistical dispersion theories are provided by Bear (1969) and Dullien (1979).

A rigorous alternative to these *ad hoc* statistical models entails generalizing the original Taylor–Aris theory to two- and three-dimensional spatially periodic models of porous media so as to encompass more complex geometries than those described by the one-dimensional constricted tube model. This approach was outlined by Brenner (1978, 1980), Lee (1979), Brenner and Adler (1982) and Dill and Brenner (1983) for inert solutes, and by Shapiro and Brenner (1988) and Dungan *et al.* (1990) for chemically reactive solutes. This multi-dimensional, spatially periodic model allows the solute mean velocity and dispersivity (as well as other macroscale solute transport properties) to be rigorously expressed in terms of the mean fluid velocity and microscale geometrical and physico-chemical properties of the system. The advantage of such *deterministic* approaches to hydrodynamic dispersion lies in the achievement of a complete and detailed understanding of the functional relations existing between the micro- and macroscale transport processes. This requires that one specify a detailed microscale geometry to characterize the porous microstructure. The degree of geometric complexity that one is able to choose in attempting to simulate real (i.e. disordered) porous media is limited only by the existing capacities of modern computers. Such deterministic models of transport processes in porous media contrast markedly with statistical approaches to the description of such phenomena, which are fundamentally founded upon a number of *ad hoc* statistical assumptions (Bear, 1969) regarding the macroscale behaviour of the system.

The practical implementation of these multi-dimensional spatially periodic models is computationally nontrivial. In this context, Lee (1979) applied a Fourier transform analysis to calculate the dispersivity of a solute flowing through a cubic array of spheres. While he was able to numerically calculate the effective solute diffusivity when convection was absent, his calculational method proved inefficacious when the characteristic microscale Péclet number (based upon unit cell size)

exceeded unity. More recently, Eidsath *et al.* (1983) applied the theory of Carbonell and Whitaker (1983) to numerically investigate dispersion accompanying solute transport during low Reynolds number flow through two-dimensional spatially periodic arrays of circular cylinders. Eidsath and co-workers employed finite-element techniques to calculate the dispersivity tensor for square and staggered arrays. While their numerical calculations were reported to be somewhat 'crude' (see also the discussion in Section 6), comparison of their results with available experimental data nevertheless allowed them to infer certain qualitatively correct conclusions as to the influence of the microscale Péclet number upon solute dispersivity.

The respective merits of spatially periodic vs completely disordered geometric models (Koch *et al.*, 1989) in quantifying dispersion phenomena arising from microscale convective-dispersive-reactive transport processes remains yet to be fully assessed in real, that is 'densely packed', porous media.

In this study we shall employ generalized Taylor dispersion theory (Brenner, 1980) to numerically determine the phenomenological coefficients characterizing the coarse-scale transport of inert solutes in two-dimensional spatially periodic models of porous media, composed of arrays of circular cylindrical bed particles. (The calculations performed in this study are based upon the microscale calculations (Edwards *et al.*, 1990a) of the Navier–Stokes interstitial velocity fields existing in these cylindrical arrays.) In particular, finite element methods are used to determine the longitudinal and lateral dispersivity coefficients for square, staggered and hexagonal arrays of circular cylinders (at various porosities) as functions of microscale Péclet and Reynolds numbers. A comparison is made of these two-dimensional numerical data with available theoretical and experimental results, the latter having been obtained however for *three-dimensional* packed beds.

In a compansion study (Edwards *et al.*, 1990b) we use these same geometric models to calculate the Darcy-scale phenomenological properties of a *reactive* solute undergoing a first-order irreversible reaction at the surfaces of the cylindrical bed particles.

2. Spatially Periodic Porous Media

Consider an unconsolidated, i.e granular, three-dimensional spatially periodic array of circular cylinders, such as is depicted in Figure 1. Solvent flows with mean velocity $\bar{\mathbf{V}}$ through the interstices of this model porous medium in a direction perpendicular to the cylinder axes, which cylinders are each of infinite length; hence any two-dimensional cross-section parallel to the plane of flow may be viewed as representative of the three-dimensional lattice. This two-dimensional periodic cross-section may be decomposed geometrically into an infinite sequence of repetitive unit cells which replicate themselves indefinitely in each of two orthogonal directions, defined here by the unit basis vectors $\mathbf{i}_1$ and $\mathbf{i}_2$, with $\mathbf{i}_1 \cdot \mathbf{i}_2 = 0$. Figure 2 depicts the particular unit cell configurations investigated in this study.

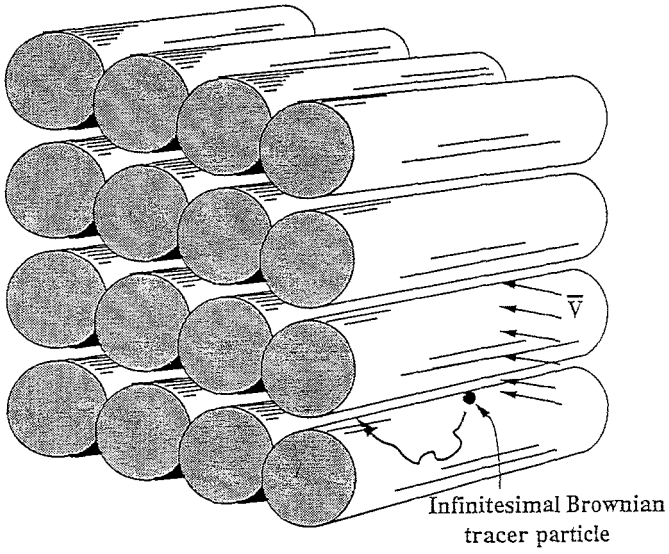

Fig. 1. A Brownian tracer particle convects and diffuses through the interstices of a model porous medium composed of an array of parallel, circular cylinders of infinite length.

Lattice points of the array, located at the geometric center of each unit cell, are defined by the denumerably-infinite set of position vectors $\mathbf{R}_n$, where $\mathbf{R}_n = \mathbf{l}_1 n_1 + \mathbf{l}_2 n_2$, with $(\mathbf{l}_1, \mathbf{l}_2)$ basic lattice vectors collinear with the orthogonal basis vectors $(\mathbf{i}_1, \mathbf{i}_2)$, respectively, and which act to define the linear dimensions, $l_1 = |\mathbf{l}_1|$ and $l_2 = |\mathbf{l}_2|$, of a rectangular unit cell (see Figure 2); (n_1, n_2) are positive or negative integers, including zero. The volume of a primitive unit cell is denoted by τ_0, which symbol also describes the entire domain within the unit cell. The intercellular domain as well as its volume are denoted by τ_f, whence the porosity of the model porous medium is simply

$$\varepsilon = \tau_f / \tau_0. \tag{2}$$

A local position vector $\mathbf{r}$ originates at the lattice point of each unit cell, such that a global position vector $\mathbf{R}$ anywhere within the infinite array may be identified as

$$\mathbf{R} = \mathbf{R}_n + \mathbf{r}, \tag{3}$$

with $\mathbf{R}$ measured from the center $(\mathbf{0})$ of an arbitrarily-chosen reference unit cell.

The numerical solution of the problem posed for the spatially periodic, (generally nonzero Reynolds number) Navier–Stokes, solvent velocity field $\mathbf{v} \equiv \mathbf{v}(\mathbf{r})$ within the interstices of the three, circular-cylindrical model porous media depicted in Figure 2, is discussed at length by Edwards *et al.* (1990a).

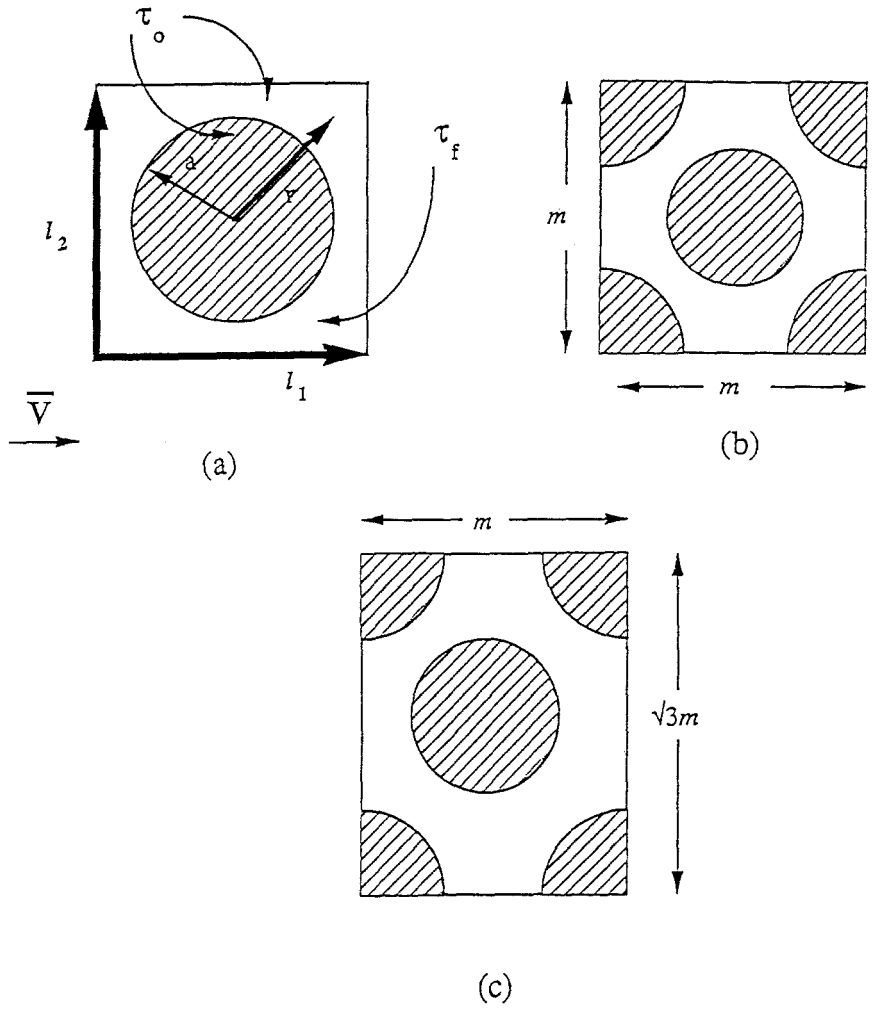

Fig. 2. Two-dimensional cross-sectional representations of the unit cell geometry for: (a) simple square array; (b) staggered array; (c) hexagonal array.

3. Mean Solute Velocity and Dispersivity

The mean solute velocity vector and dispersivity dyadic for macroscopically unidirectional incompressible flows through spatially periodic porous media were first calculated by Brenner (1978, 1980), who employed a method-of-moments scheme. This solution scheme yields the mean *solute* velocity vector $\bar{\mathbf{U}}^*$, which is identical with the mean interstitial *solvent* velocity vector $\bar{\mathbf{V}}$, namely

$$\bar{\mathbf{U}}^* = \bar{\mathbf{V}} \equiv \frac{1}{\tau_f} \int_{\tau_f} \mathbf{v}(\mathbf{r})\, d^3\mathbf{r}, \tag{4}$$

at least for the class of nonreactive solutes considered in this paper. The same

scheme furnishes the solute dispersivity dyadic in the form

$$\bar{\mathbf{D}}^* = \frac{D}{\tau_f} \int_{\tau_f} \nabla \mathbf{B}^\dagger \cdot \nabla \mathbf{B} \, \mathrm{d}^3\mathbf{r}, \tag{5}$$

with $\nabla \equiv \partial/\partial \mathbf{r}$ the intracellular gradient operator. The vector field $\mathbf{B}(\mathbf{r})$ appearing in the above integrand represents the solution of the following unit cell boundary-value problem:

$$-\mathbf{v} \cdot \nabla \mathbf{B} + D\nabla^2 \mathbf{B} = \bar{\mathbf{U}}^*, \tag{6}$$

subject to the boundary condition

$$v \cdot \nabla \mathbf{B} = \mathbf{0} \quad \text{on } S_p, \tag{7}$$

with S_p the bed-particle surface(s) within the cell and v a unit normal vector on S_p. Additionally, $\mathbf{B}$ is to satisfy the pair of jump conditions

$$[[\mathbf{B}]] = [[\mathbf{r}]], \qquad [[\nabla \mathbf{B}]] = \mathbf{0} \tag{8a, b}$$

across opposite cell faces, where the 'jump' in the value of the generic field $\mathbf{f}$ is defined as $[[\mathbf{f}]] = \mathbf{f}(\mathbf{r} + \mathbf{l}_j) - \mathbf{f}(\mathbf{r})$.

By introducing the transformation

$$\hat{\mathbf{B}} = \mathbf{B} + \mathbf{r} + \text{const.}, \tag{9}$$

a computationally more useful form of the $\mathbf{B}(\mathbf{r})$-field equation obtains in the form of the unit cell boundary-value problem

$$\nabla \cdot (\mathbf{v}\hat{\mathbf{B}}) - D\nabla^2 \hat{\mathbf{B}} = \mathbf{v} - \bar{\mathbf{U}}^*, \tag{10}$$

to be solved in the interstitial unit cell domain $\mathbf{r} \in \tau_f$ subject to the 'boundary' conditions

$$v \cdot \nabla \hat{\mathbf{B}} = v \quad \text{on } S_p, \tag{11}$$

$$[[\hat{\mathbf{B}}]] = \mathbf{0}, \qquad [[\nabla \hat{\mathbf{B}}]] = \mathbf{0}. \tag{12a, b}$$

Numerical solution (for various model porous media geometries, see Figure 2) of the problem posed by Equations (10)–(12) for $\hat{\mathbf{B}}(\mathbf{r})$ constitutes an intermediate objective of this study, knowledge of which field ultimately permits the dispersivity dyadic to be obtained from (5).

This $\hat{\mathbf{B}}(\mathbf{r})$-field problem is equivalent to the comparable $\mathbf{f}$-field problem formulated by Eidsath *et al.* (1983) [see their Equations (46), (47)], which field they subsequently used for calculations of the dispersivity tensor. This tensor appears in the macroscopic solute transport equation, the form of which is unique, as predicted by Brenner (1980) and Carbonell and Whitaker (1983).

The conditions embodied in Equations (12) are essential for the proper definition, and ultimately the solution, of the $\hat{\mathbf{B}}$-field problem (which field is, however, uniquely determined only to within an arbitrary constant). These conditions are

rigorously derived (Brenner, 1980) from the 'method-of-moments' scheme, which stands in contrast to the *ad hoc* volume-averaging theory of Carbonell and Whitaker (1983). Although the latter theory reproduces the same results as the Taylor–Aris method of moments, it was allegedly developed for an arbitrary (e.g. wholly disordered) porous medium. In fact, their **f**-field problem – posed within the fluid domain of the 'averaging volume' V_β of the arbitrary porous medium [cf. their Equations (35), (36)] – is not uniquely defined without imposing appropriate boundary conditions on the external boundaries of V_β. Eidsath *et al.* (1983), when considering the **f**-field problem posed for a unit cell of a spatially periodic medium, "...ignore the [above-mentioned] condition at the entrances and exits..." of the unit cell, *intuitively* replacing them with periodicity conditions equivalent to (12).

4. Method of Solution

A finite element numerical scheme was used to solve Equations (10)–(12), employing biquadratic Langrangian interpolation for the $\hat{\mathbf{B}}$ field, and using an isoparametric element type. The acutal meshes used in this study, each composed of 400 nine-node elements, were identical to those discussed by Edwards *et al.* (1990a). The maximum value of the element Péclet number did not exceed 50, even for the largest values of the cylinder Péclet number $\mathrm{Pe} = 2\bar{V}a/D$. The whole cylinder surface was composed of 72 piecewise continuous parabolic arches, which number allowed sufficiently accurate calculations of the velocity (i.e. **v**) and $\hat{\mathbf{B}}$ fields. Comparisons with known analytical and numerical solutions indicated a good fit, with deviations being less than 2.5%. For further details the reader is referred to the article of Edwards *et al.* (1990a).

The vector boundary-value problem posed above possesses unique features in relation to the more conventional scalar convective-diffusive-type equation extensively discussed in the finite element literature (see, for example, Hughes, 1987). However, the individual scalar components of the vector equation (10) may each be viewed as fully separate convection-diffusive problems in the presence of the (prescribed) distributed source vector density $\mathbf{v} - \bar{\mathbf{U}}^*$.* We adopted this linearly independent decomposition by solving separately for the longitudinal and lateral components (the former colinear with $\mathbf{l}_1$ in Figure 2 and parallel to the mean fluid velocity vector $\bar{\mathbf{V}}$).

The systems of linear algebraic equations resulting from the finite element formulation were solved using a skyline block storage mode with a direct triangular decomposition scheme. As with the comparable fluid dynamic problem (Edwards *et al.*, 1990a), periodicity conditions were imposed by identifying appropriate pairs of nodes as constituting the same node along the periodic boundaries.

The problem posed by Equations (10)–(12) proved overly stiff in the most general case to admit direct computation (numerical instabilities being observed near the cylindrical bed particle surfaces). This stiffness arises from the fact that the

*Note that as a consequence of (4) the mean source strength is identically zero, i.e. $\tau_f^{-1} \int_{\tau_f} [\bar{\mathbf{U}}^* - \mathbf{v}(\mathbf{r})]\, d^3\mathbf{r} = \mathbf{0}$. Hence, though each component of the $\hat{\mathbf{B}}$ field is not 'conserved' locally at point **r**, each is nevertheless conserved *en toto*; that is, on average, the net source and sink strengths vanish.

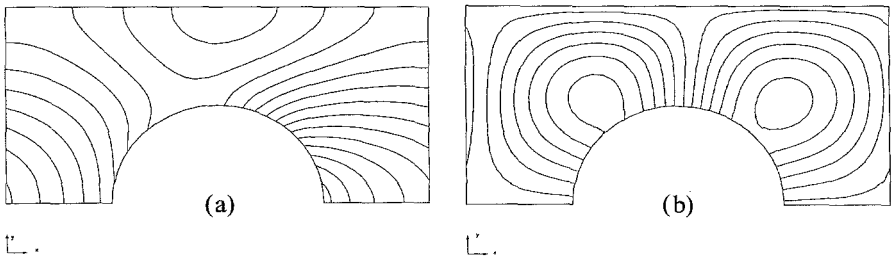

Fig. 3. Illustrative $\hat{\mathbf{B}}$-field contours for the simple square array, with Pe = 1 and $\varepsilon = 0.804$; (a) $\hat{B}_x$ component; (b) $\hat{B}_y$ component.

$\hat{\mathbf{B}}$-field solution is uniquely determined only to within an arbitrary constant vector (Brenner, 1980). To avoid instability in the numerical solution it was found necessary to add to $\bar{\mathbf{U}}^*$ in (10) a time-dependent $\partial\hat{\mathbf{B}}/\partial t$ term, essentially with the purpose of iterating toward a solution of the original time-independent boundary-value problem (10)–(12). As shown by Edwards *et al.* (1990b), the long-time solution of this new partial differential equation, subject to (11) and (12), is identical with that of (10) (to within an arbitrary, additive time-dependent constant vector). The $\hat{\mathbf{B}}$-field solution is thus approached iteratively, in each case requiring less than eight time iterations to achieve convergence; $\hat{\mathbf{B}}$-field contours for the particular case of Pe = 1 and $\varepsilon = 0.804$ are illustrated in Figure 3. It may be seen that the lines of constant $\hat{B}_x$ and $\hat{B}_y$ are smooth, not exhibiting the characteristic wavy behavior typical of numerical instabilities (Hughes, 1987).

The longitudinal and lateral components of the $\hat{\mathbf{B}}$-field determined in this manner were subsequently used to numerically evaluate the integral (5) governing the longitudinal and lateral components of the dispersivity dyadic. This was done by Gaussian integration performed locally over each element.

4.1. PURE MOLECULAR DIFFUSION: ANALYTICAL-NUMERICAL COMPARISON

To test the accuracy of our numerical solution against a known limiting case, for which analytical results are available, we applied the above numerical formulation to the case of pure diffusion in a two-dimensional, simple array of circular cylinders, where the solute tracer is free to diffuse within both the fluid and solid phases, as shown in Figure 4. Numerical results for this diffusively-isotropic case are presented in Table I in terms of a composite or effective molecular diffusivity $\bar{D}$ as a function of the porosity ε and diffusivity ratio $\alpha = D_d/D_c$, with D_d and D_c the respective dispersed- and continuous-phase diffusivities.

The problem of calculating composite-media effective diffusivities dates back to the classical studies of Maxwell (1873) and Rayleigh (1892). More recently, Perrins *et al.* (1979) furnished a complete, theoretical solution of the effective conductivity problem for circular cylinders, valid over the entire range of ε and α. The comparison in Table I of our numerical results with theirs, displays excellent agreement for all values of these parameters, thereby providing confidence in the accuracy of our numerical approach.

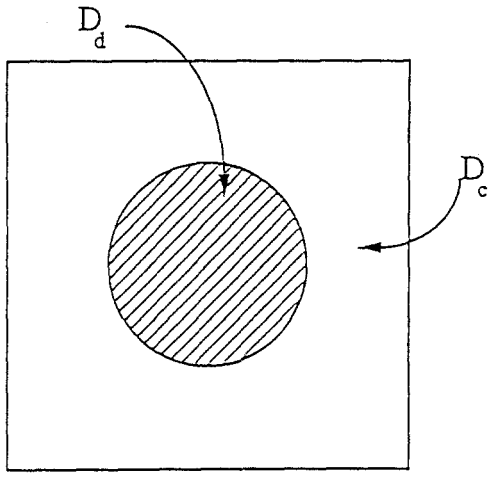

Fig. 4. A unit cell composed of a circular cylinder through which solute diffuses with diffusivity D_d, and an interstitial phase through which solute diffuses with diffusivity D_c.

Table 1. Comparison between the composite diffusivity $\bar{D}$ of a simple square array of cylinders determined numerically and the analytical results of Perrins *et al.* (1979), as a function of dispersed phase volume fraction ε and microscale diffusivity ratio $\alpha = D_d/D_c$.

ε	α	$\bar{D}/D_c$ Numerical	Perrins *et al.* (1979)
0.804	2	1.1401	1.1399[a]
0.804	10	1.3829	1.3827[a]
0.599	2	1.3086	1.3089[a]
0.599	10	1.9833	1.9849[a]
0.406	2	1.4963	1.4965[a]
0.406	10	2.9910	2.9961[a]
0.288	2	1.6302	1.6278[a]
0.288	10	4.2437	4.2440[a]
0.230	2	1.7022	1.7023
0.230	10	5.4659	5.4674

[a]Interpolated data

4.2. CONVECTIVE-DIFFUSION BETWEEN PARALLEL CORRUGATED PLATES

As a second verification of our numerical scheme, we have calculated the longitudinal dispersivity for flow between two parallel plates, separated by a distance $2h$ and possessing half-cylinder corrugations of radii a, as in Figure 5. Figure 6 shows the results of this calculation for three values of the ratio $a/2h$, together with a comparison of these numerical values with the limiting analytical, flat-plate result

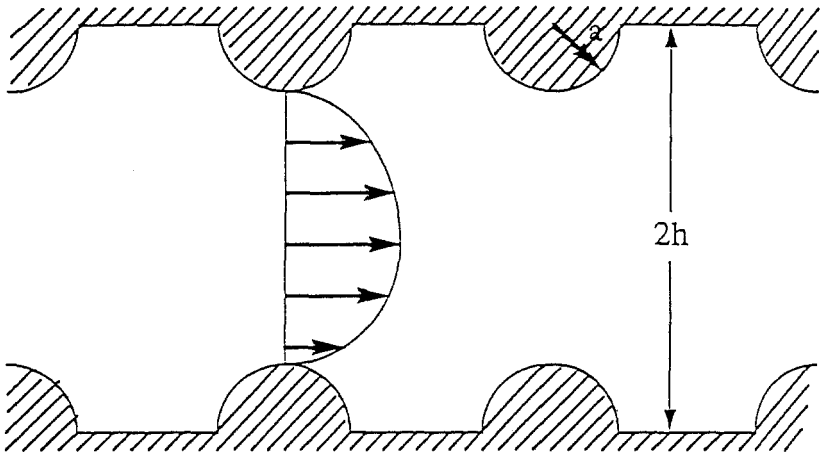

Fig. 5. Flow between two parallel plates separated by a distance $2h$, with evenly-spaced, semi-circular protrusions (of radii a) along the plates.

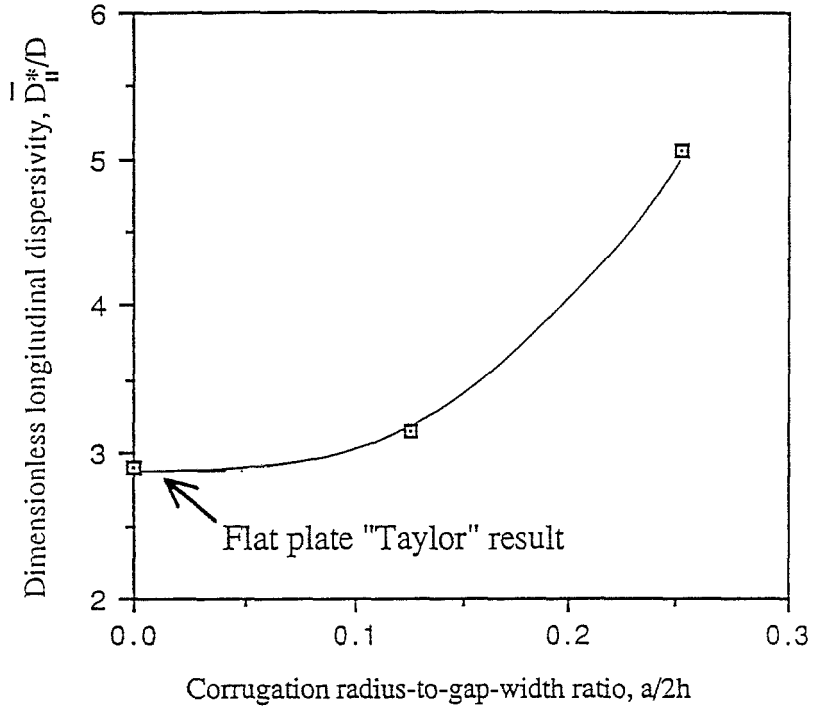

Fig. 6. Comparison of the current longitudinal dispersivity numerical results for the geometry of Figure 5, with the limiting parallel-plate result of Wooding (1960) in the absence of protrusions.

(Wooding, 1960) for $a/2h = 0$,

$$\frac{\bar{D}^*_{\parallel}}{D} = 1 + \frac{\mathrm{Pe}^2}{210}, \tag{13}$$

with $\mathrm{Pe} = 2h\bar{V}/D$. The agreement of our (extrapolated) numerics with the analytical limit of Wooding (1960) is observed to be quite satisfactory.

5. Dispersivities for Square, Staggered and Hexagonal Arrays

Displayed in Table II are numerically calculated longitudinal and lateral dispersivities for square, staggered and hexagonal arrays as functions of bed porosity ε, microscale Péclet number, $\mathrm{Pe} = 2a\bar{V}/D$ and Reynolds number $\mathrm{Re} = 2a\rho\bar{V}/\mu$.

5.1. EFFECT OF PACKING ARRANGEMENT

The longitudinal dispersivity constitutes the dominant component of the dispersivity dyadic, especially at the larger Péclet numbers. This is to be expected since the corresponding component of the fluid velocity, parallel to the mean flow direction, exhibits the most significant gradients. This effect is, however, less pronounced for

Table II. Nondimensional numerical values of the longitudinal ($\bar{D}^*_{\parallel}$) and the lateral ($\bar{D}^*_{\perp}$) dispersivities as functions of bed porosity, Reynolds and Péclet numbers for square, hexagonal and staggered arrays of circular cylinders

			Square array		Hexagonal array		Staggered array	
ε	Re	Pe	$\bar{D}^*_{\parallel}/D$	$\bar{D}^*_{\perp}/D$	$\bar{D}^*_{\parallel}/D$	$\bar{D}^*_{\perp}/D$	$\bar{D}^*_{\parallel}/D$	$\bar{D}^*_{\perp}/D$
0.804	0	0	0.8357	0.8357	0.7823	0.7823		—
0.804	0	1	0.9464	0.8440	0.8403	0.8328	—	—
0.804	0	10	6.0692	0.9746	4.3465	1.0469	—	—
0.804	0	100	301.76	1.2164	215.47	1.3751	—	—
0.804	20.9	100	644.82	1.1259	—	—	—	—
0.804	100	100	868.47	0.9906	—	—	—	—
0.804	0	1000	17,754.7	1.7139	18,955.6	1.8328	—	—
0.804	20.9	1000	56,641.3	1.2439	—	—	—	—
0.804	100	1000	67,687.7	1.4892	—	—	—	—
0.599	0	0	0.7095	0.7095	0.7135	0.7135	0.7085	0.7085
0.599	0	1	0.8605	0.7112	0.7753	0.9775	0.7216	0.8495
0.599	0	10	7.1223	0.8062	4.2237	1.1930	1.5403	1.9607
0.599	0	100	359.37	1.0100	176.53	1.6662	48.8357	2.8567
0.599	0	1000	26,921.8	1.2413	14,299.9	2.0813	4330.56	3.6340
0.400	0	0	—	—	—	—	—	—
0.400	0	1	0.9368	0.5728	0.6390	0.6371	—	—
0.400	0	10	10.356	0.6130	1.5613	0.8547	—	—
0.400	0	100	524.54	0.7038	57.734	1.0839	—	—
0.400	0	1000	34,576.7	0.8188	3246.39	1.3828	—	—

staggered and hexagonal arrays, where the streamlines show more tortuous curvilinear patterns (Edwards *et al.*, 1990a). Consequently, the average direction of the largest velocity gradients deviates from that prevailing for the simple square array. As a result, all other things being equal, the longitudinal dispersivities of the hexagonal array and especially of the staggered array (for which the curvilinear character of the streamlines is most pronounced) are less than those of the square array.

Opposite trends are exhibited by the lateral dispersivity. At large Péclet numbers, the main contribution to this dispersivity component is apparently due to the lateral fluid motion (Edwards *et al.*, 1990a) existing within the unit cell. Since the magnitude of such transverse fluid motion is largest for the staggered array geometry, the latter attains the largest lateral dispersivity. On the other hand, the intercellular lateral fluid motion in the square array is confined to the regions between the cylinders, where the flow occurs along closed streamlines. Since this motion is relatively weak (Edwards *et al.*, 1990a), the resulting lateral dispersivity is less than that for the hexagonal array.

5.2. EFFECT OF POROSITY

Table II shows that diminishing void fraction results in a sharp increase in longitudinal dispersivity for the square array. This effect may be explained by the existence of increasingly large velocity gradients in the gap between the cylinders, where the local velocity vector is primarily in the direction of the mean flow. On the contrary, for the hexagonal (and staggered) arrays, which exhibit a more tortuous flow path, decreasing porosity results in reorientation of the local fluid velocity in the lateral direction, resulting in a decrease in the longitudinal dispersivity.

Lateral dispersivities for the square and hexagonal arrays also diverge (Table II) in their respective trends with decreasing bed porosity. For the square array this dispersivity component decreases with decreasing ε, whereas for the hexagonal array it goes through a maximum, all other things being equal; this differing behavior may be explained by the diminished number of closed intercellular fluid streamlines for the square array compared with those for the hexagonal array.

5.3. EFFECT OF PÉCLET NUMBER

A general correlation of the variation of longitudinal dispersivity with Péclet number may be inferred from Figures 7 and 8, where the longitudinal dispersivities for square and hexagonal arrays are plotted on a logarithmic scale vs Péclet number (for $\mathrm{Pe} > 10$) at various parameters of the bed porosity ε, and for a zero Reynolds number. Application of a least-squares analysis to these data leads to a correlation of the form

$$\bar{D}^*_{\parallel}/D = A\,\mathrm{Pe}^m, \tag{14}$$

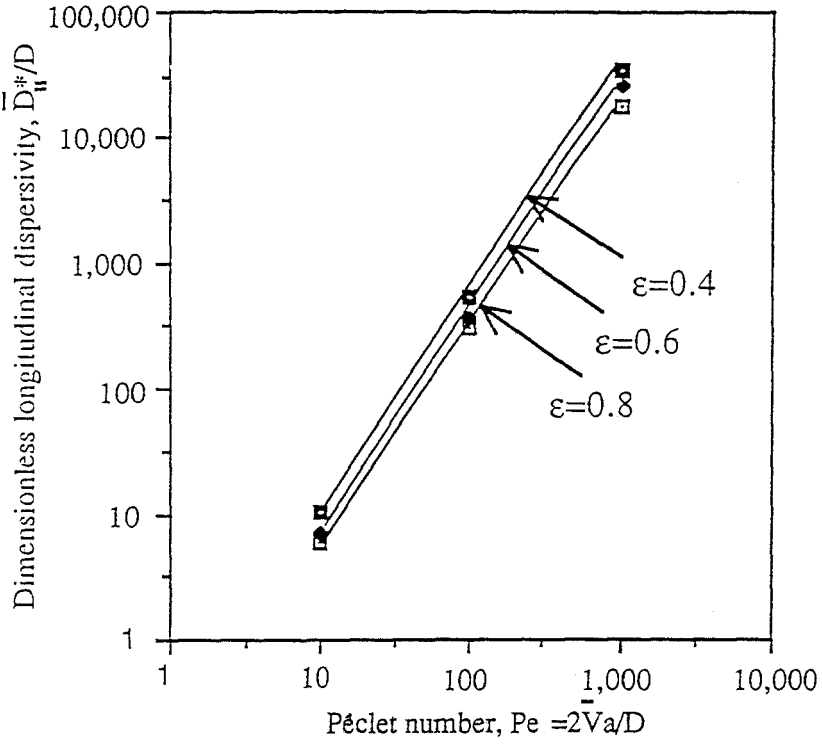

Fig. 7. Dimensionless longitudinal dispersivity of a square array of cylinders vs Péclet number for three values of the porosity.

with values of the coefficients A and m displayed in Table III. Average values of the coefficients for all three arrays are also shown. The approximate value of 1.7 for the exponent in (14) accords with that suggested by Eidsath *et al.* (1983) based upon their numerical dispersivity calculations for square and staggered cylindrical arrays. (Their work is discussed at length in the following section.)

Table III. Least-squares regression coefficients for Equation (14) at Re = 0

	Square array		Hexagonal array	
ε	A	m	A	m
0.804	0.109	1.734	0.0594	1.820
0.599	0.109	1.789	0.0650	1.765
0.400	0.174	1.760	0.0319	1.659
Average	0.130	1.761	0.0520	1.748

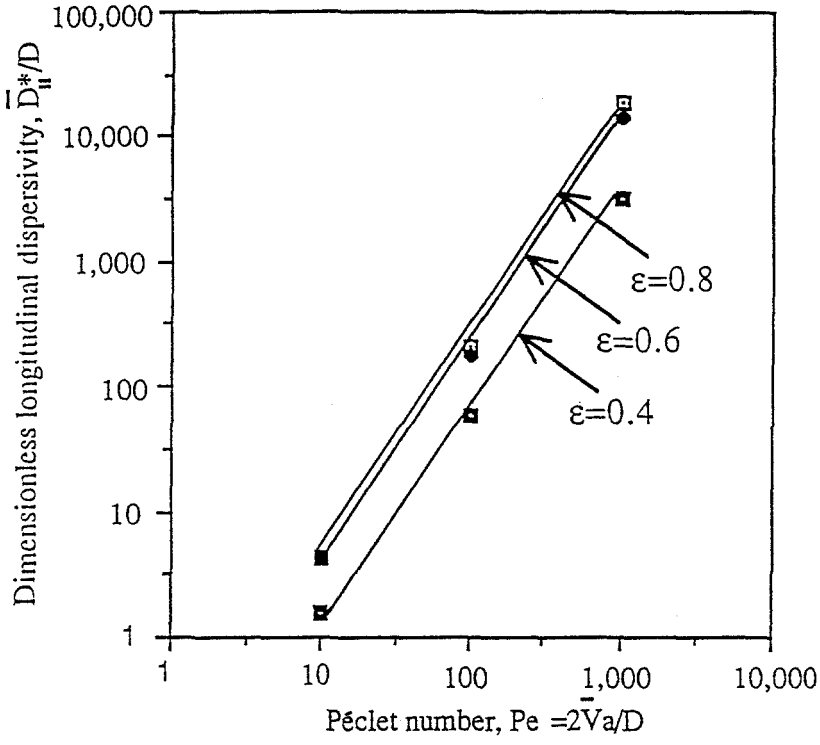

Fig. 8. Dimensionless longitudinal dispersivity of a hexagonal array of cylinders vs Péclet number for three values of the porosity.

5.4. EFFECT OF REYNOLDS NUMBER

Reynolds number effects are shown in Table II, for the square array at $\varepsilon = 0.8$, and for $Pe = 100$ and $Pe = 1000$. A dramatic increase in the longitudinal dispersivity with Re is evident, one whose origin can be attributed to the intracell fluid flow redistribution, resulting in the creation of a linear streamline zone in the gap between cylinders (Edwards *et al.*, 1990a). Due to this effect, the microscale velocity distribution in the latter region resembles a classical (Wooding, 1960) rectilinear flow occurring between parallel plates. This phenomenon results in a tendency towards a classical Pe^2 dependence of $\bar{D}^*_{\parallel}$ upon Péclet number with increasing values of the latter (for *all* porosities).

In contrast with the above-cited behavior, the lateral dispersivity diminishes with increasing Re as a result of the above redistribution.

6. Comparison with Previous Theoretical and Experimental Data

6.1. LONGITUDINAL DISPERSIVITY

Eidsath *et al.* (1983), using a finite element numerical method, presented longitudinal dispersivity results for square and staggered cylindrical arrays with $\varepsilon = 0.37$. For

Table IV. Comparison of numerical values of the dimensionless longitudinal dispersivity for simple square arrays of cylinders calculated by the current study with values calculated by Eidsath *et al.* (1983) for $\varepsilon = 0.37$ and $\mathrm{Re} = 0$

Pe_p	Current results $(\bar{D}^*_{\parallel}/D)$	Eidsath *et al.* (1983) $(\bar{D}^*_{\parallel}/D)$
0.403	0.7846	0.616
0.59	0.9684	—
4.03	6.0635	2.44
5.9	10.927	—
40.31	282.3	80.56
58.5	555.40	—
303	10,667.8	—
403.1	16,928	4,652
2,015.6	191,474	89,219

the sake of comparison we have for the same porosity computed the dispersion coefficients via our own scheme. These dispersivities are reported in Table IV, together with the corresponding results of Eidsath (1981). The dispersivity values of Eidsath and co-workers, which are reported in Table IV vs the particle Péclet number

$$\mathrm{Pe}_p \overset{\text{def}}{=} \frac{2a\bar{V}}{D}\frac{\varepsilon}{1-\varepsilon} \tag{15}$$

used in their work, are seen to be several-fold smaller than ours. Moreover, Eidsath *et al.* found that dispersion increases only 'slightly' with increasing Reynolds number; explicitly, Eidsath (1981) reported an increase of about 10% in the longitudinal dispersivity of a staggered array (possessing a porosity of $\varepsilon = 0.365$) when Re increased from 0.006 to 56. Our results for $\varepsilon = 0.804$, however, indicate a significant effect of fluid inertia upon solute dispersivity. Indeed, as may be observed from Table II, increasing Re from 0 to 100 leads to a 3 to 4-fold increase in the longitudinal dispersivity. Normally, since $\mathrm{Pe} = \mathrm{Re}\, v/D$, the Pe and Re numbers both increase in unison in dispersion experiments performed with a given solute and fluid. Therefore, in order to experimentally investigate the effect of Reynolds number alone upon solute dispersivity, one should compare experimental data obtained for different fluids, e.g. for air and water, or different solutes. Such a comparison of the results of Han *et al.* (1985) with those of Gunn and Pryce (1969), both obtained for $\mathrm{Pe} = 136$ and the respective values of $\mathrm{Re} = 107$ and 0.36, indicate only a 50% change in the longitudinal dispersivity, which lies within the range of accuracy of both experimental results. One should note, however, that the above data were obtained for beds composed of different particles, and may therefore correspond to significantly different bed microstructures.

Possible sources of disagreement between the present results and those of Eidsath *et al.* (1983) may be contemplated: (i) The latter study employed a 36-element

mesh, whereas we used a 400-element mesh for the same fluid domain; (ii) Eidsath *et al.* employed a subparametric element type, which is unable to conform to the cylindrical boundaries, whereas we employed an isoparametric element, which is conformable; (iii) whereas we approached the $\hat{\mathbf{B}}$-field solution iteratively to avoid numerical instabilities, irregularities of the **f**-field pattern reported in the work of Eidsath (1981) suggest that such instabilities were actually observed in the latter study.

Figure 9 compares theoretical and experimental longitudinal dispersivities collected from several sources with present numerical results. It may be seen that the experimental data of Gunn and Pryce (1969), measured for cubic arrays of spheres, lies somewhat between the two curves respectively calculated for square and hexagonal arrays of cylinders. This observation cannot, however, constitute a verification of the accuracy of our *two-dimensional* analysis, since the above experiments pertain to *three-dimensional* arrays. For small values of the Péclet number the two packing arrangements yield similar values of $\bar{D}^*_{\parallel}$, thereby suggesting that solute dispersion in this region is dominated by molecular diffusion.

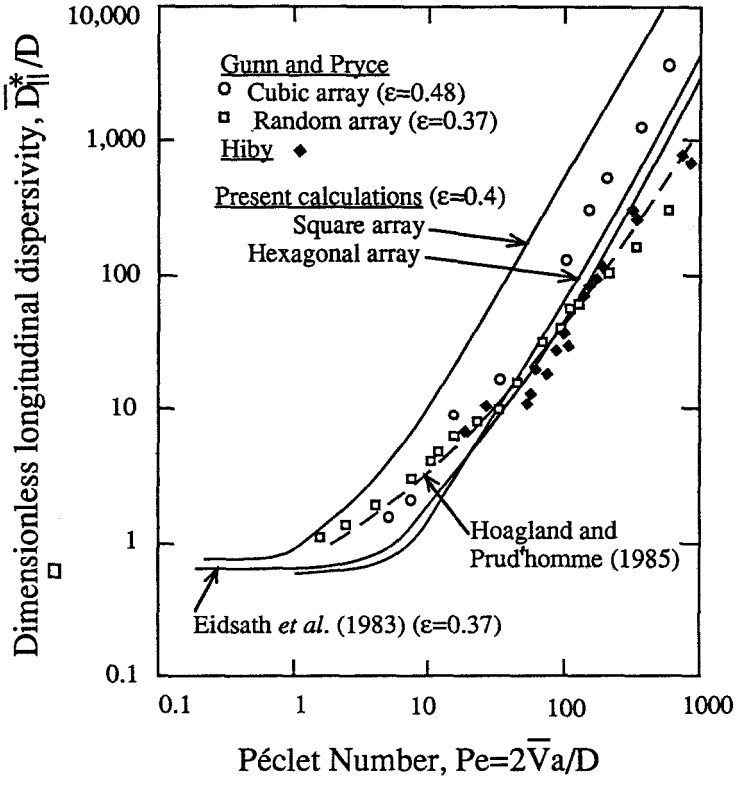

Fig. 9. Comparison of the experimental data of Gunn and Pryce (1969) and the data of Hiby (1962) with the numerical results of Eidsath *et al.* (1983), the sinusoidal-tube model of Hoagland and Prud'homme (1985), and the current numerical results.

However, the results of Gunn and Pryce (1969) indicate that the longitudinal dispersivity is independent of the array's microstructure over a much wider Pe range. Indeed, one can observe that randomly packed beds and cubic arrays of spherical particles yield similar dispersivities up to $\mathrm{Pe} = 20$, beyond which value the dispersivity of an ordered array is larger.

As may further be seen from Figure 9, the numerical calculations of Eidsath *et al.* (1983) predict significantly smaller longitudinal dispersivities than do we for the square array, although these dispersivities fit our data calculated for the hexagonal array. The sinusoidal tube model of Hoagland and Prud'homme (1985) accords well with the data of Hiby (1962) measured for disordered arrays. While the data of Eidsath *et al.* is calculated for a bed porosity of $\varepsilon = 0.37$, it is not possible to unambiguously assign a specific ε value to the data of Hoagland and Prud'homme (1985). If it is supposed, however, that their constricted tubes are packed into a square array, the porosity may be shown to be 0.433 – close to the ε values characterizing the other data shown in Figure 9. It is further seen that the experimental data of Hiby [cited by Hoagland and Prud'homme (1985)] for granular beds displays significantly lower longitudinal dispersivities than does that of Gunn and Pryce (1969); yet each shows a similar slope, characterized by the exponent $n = 1.2$ in Equation (14). The discrepancy existing among the several experimental data sets may be attributed to differences in bed microstructure, which structure can significantly affect the magnitude of the dispersivity (Han *et al.*, 1985). The numerical dispersivity results obtained in our work support this statement, especially for small bed voidages. As such, one can perhaps choose that particular microscale packing arrangement which furnishes a longitudinal dispersivity most closely fitting the experimental data. In this respect we note that longitudinal dispersivities calculated by the present model for the staggered array would more closely approach the data of Hiby and of Gunn and Pryce measured for random arrays.

Existing experimental *three-dimensional* dispersivity data cannot strictly support (or negate) *two-dimensional* models of the type considered here. We thus disagree with the conclusions of Eidsath *et al.*, who interpreted the observed 'fit' between their two-dimensional numerical results and Gunn and Pryce's (1985) experimental data as supporting the original volume-averaging theory of Carbonell and Whitaker (1983). Nor may the data obtained for various microscale (spatially periodic) packing arrangements be interpreted as an 'effect of randomness' of the porous medium, as Eidsath *et al.* (1983) claim. A more objective comparison between numerical and experimental data can possibly be provided by measurements of both longitudinal and lateral dispersivities in two-dimensional fibrous beds, with the fibers oriented perpendicular to the mean flow direction. More practically useful, however, would be the numerical solution of *three*-dimensional convective-dispersion models (e.g. of arrays of spheres), which could be compared with the numerous experimental data available (Rifai *et al.*, 1956; Carbery and Bretton, 1958; Ebach and White, 1958; Edwards and Richardson, 1968; Blackwell *et al.*, 1959; Fried and Combarnous, 1971; Dullien, 1979).

6.2. LATERAL DISPERSIVITY

We found the lateral dispersivities reported in Table II to be several-fold less than the experimental ones, especially at the larger Péclet numbers; this observation is similar to the findings of Eidsath *et al.* This discrepancy may be understood by noting that the intercellular lateral fluid motion (which strongly affects this dispersivity component) is relatively weak. Consequently, the lateral solute dispersion is actually governed by the slow molecular diffusion process occurring at the unit cell boundaries. Eidsath *et al.*, while pointing out that the spatially periodic porous medium models possess limited merits in predicting lateral dispersivities, attribute this discrepancy to the existence of local heterogeneities in real porous media. Further theoretical investigations of lateral dispersion in arrays characterized by more complex intracell geometries (as well as parametric investigations of the orientation effect of the fluid's mean velocity vector $\bar{\mathbf{V}}$ relative to the lattice axes) are needed to provide a more complete answer to this question.

7. Conclusions

Numerically calculated longitudinal and lateral dispersivity values have been provided for square, staggered and hexagonal two-dimensional arrays of circular cylinders as functions of bed porosity as well as of Péclet and Reynolds numbers. These finite element numerical results, which compare favorably with theoretical results obtained by Perrins *et al.* (1979) in the limiting case of pure molecular diffusion, indicate that the longitudinal dispersivity $\bar{D}^*_{\parallel}$ generally increases with Péclet number at a rate less than Pe^2. With increasing Péclet number, however, a Pe^2 dependence is approached asymptotically. The longitudinal dispersivity strongly depends upon the bed packing arrangement, with the square array exhibiting the largest $\bar{D}^*_{\parallel}$ due to the rectilinear streamline zone prevailing between the bed particles in this configuration. Increasing the Reynolds number has the effect of extending the length of the latter zone, thereby significantly enhancing longitudinal dispersion. On the other hand, increasing bed tortuosity leads to the formation of closed streamline zones, thereby reducing longitudinal dispersivity, while simultaneously enhancing lateral dispersivity. Decreasing bed porosity may either promote or inhibit longitudinal solute dispersion, depending upon the bed microstructure.

The longitudinal dispersivity values calculated in this study are several-fold larger than the numerical values reported by Eidsath *et al.* (1983). The most likely source of disagreement between the respective numerical results is the relatively inferior finite element scheme used by Eidsath *et al.*, which employed nonconforming subparametric elements jointly with an overly-sparse mesh construction.

Acknowledgements

This work was supported by the National Science Foundation and the U.S. Army Research Office (Contract No. DAAL03-87-K-0128). D.E. was supported by a

Lady Davies Fellowship. M. Shapiro acknowledges the support of the Basic Research Foundation administered by the Israel Academy of Science and Humanities and of the Technion VPR Fund – Bernstein Fund for the Promotion of Research. M. Shapira acknowledges the support of a Deutch Foundation Fellowship. We are grateful to Mr Itzchak J. Kettner for performing part of the calculations and to Professor Stephen Whitaker for his extensive comments on an earlier draft of this manuscript, as well as for furnishing us with a copy of Eidsath's thesis.

References

Aris, R., 1956, On the dispersion of a solute flowing slowly through a tube, *Proc. R. Soc. Lond.* **A235,** 67–77.

Aris, R. and Amundson, N. R., 1957, Some remarks on longitudinal mixing and diffusion in packed beds, *AIChE J.* **3,** 280–282.

Bear, J., 1969, Hydrodynamic dispersion, in R. J. M. de Wiest (ed.), *Flow Through Porous Media,* Academic, New York, pp. 109–196.

Bear, J. 1972, *Dynamics of Fluids in Porous Media*, American Elsevier, New York.

Blackwell, R. J., Rayne, J. R., and Terry, W. M., 1959, Factors influencing the efficiency of miscible displacement, *AIME Petroleum Trans.* **217**, 1–8.

Brenner, H., 1978, Dispersion resulting from flow through spatially periodic porous media, in W. Fiszdon, R. Herczynski, and M. Bratos (eds.), *Fluid Dynamics Transactions*, Vol. 9 (Polish Academy of Sciences, Institute of Fundamental Technological Research), PWN–Polish Scientific Publishers, Warsaw.

Brenner, H., 1980, Dispersion resulting from flow through spatially periodic porous media, *Phil. Trans. R. Soc. Lond.* **A297,** 81–133.

Brenner, H. and Adler, P. M., 1982, Dispersion resulting from flow through spatially periodic porous media II. Surface and intraparticle transport, *Phil. Trans. R. Soc. Lond.* **A307,** 149–200.

Carbonell, R. G. and Whitaker, S., 1983, Dispersion in pulsed systems – II. Theoretical developments of passive dispersion in porous media, *Chem. Engng. Sci.* **38,** 1795–1816.

Dill, L. H. and Brenner, H., 1983, Dispersion resulting from flow through spatially periodic porous media. III. Time-periodic processes, *Physico-Chem. Hydrodyn.* **4**, 279–302.

Dullien, F. A. L., 1979, *Porous Media: Fluid Transport and Pore Structure*, Academic, New York.

Dungan, S. R., Shapiro, M., and Brenner, H., 1990, Convective-diffusive-reactive Taylor dispersion processes in particulate multiphase systems, *Proc. R. Soc. Lond.* **A429,** 639–671.

Ebach, E. A. and White, R. R., 1958, Mixing of fluids flowing through beds of packed solids, *AIChE J.* **4**, 161–164.

Edwards, M. F. and Richardson, J. F., 1968, Gas dispersion in packed beds, *Chem. Engng Sci.* **23,** 109–123.

Edwards, D. A., Shapiro, M., Bar-Yoseph, P., and Shapira, M., 1990a, The influence of Reynolds number upon the permeability of spatially periodic arrays of cylinders, *Phys. Fluids A* **2**(1), 45–55.

Edwards, D. A., Shapiro, M., and Brenner H., 1990b, Convective dispersion in chemically reactive, spatially periodic, two-dimensional model porous media (in preparation).

Eidsath, A., 1981, Flow and dispersion in spatially periodic porous media: A finite element study, MSc thesis, University of California, Davis.

Eidsath, A., Carbonell, R. G., Whitaker, S., and Herrmann, L. R., 1983, Dispersion in pulsed systems – III. Comparison between theory and experiments for packed beds, *Chem. Engng. Sci.* **38,** 1803–1816.

Fried, J. J. and Combarnous, M. A., 1971, Dispersion in porous media, *Adv. Hydrosci.* **7,** 169–282.

Gunn, D. J. and Pryce, C., 1969, Dispersion in packed beds, *Trans. Instn. Chem. Engrs.* **47,** T341–T350.

Han, N. W., Bhakta, J., and Carbonell, R. G., 1985, Longitudinal and lateral dispersion in packed beds: Effect of column length and particle size distribution, *AIChE J.* **31,** 277–288.

Hiby, J. W., 1962, Longitudinal and transverse mixing during single-phase flow through granular beds, *Symp. Interaction between Fluids and Particles, Inst. Chem. Engrg.*, London, pp. 312–325.

Hoagland, D. A. and Prud'homme, R. K., 1985, Talyor-Aris dispersion arising from flow in a sinusoidal tube, *AIChE J.* **31,** 236–244.

Hughes, T. J. R., 1987, *The Finite Element Method*, Prentice-Hall, Englewood Cliffs, N. J.

Koch, D. L. and Brady, J. F., 1985, Dispersion in fixed beds, *J. Fluid Mech.* **154,** 399–427.

Koch, D. L., Cox, R. G., Brenner, H., and Brady, J. F., 1989, The effect of order on dispersion in porous media, *J. Fluid Mech.* **200,** 173–188.

Lee, H. L., 1979, Analysis of pseudo-continuum mass transfer in media with spatially-periodic boundaries, *Chem. Engng. Sci.* **34,** 503–514.

Maxwell, J. C., 1873, *A Treatise on Electricity and Magnetism*, Vol. 1, Clarendon Press, London.

Payatakes, A. C., Tien, C., and Turian, R. J., 1975, A new model for granular porous media, *AIChE J.* **19,** 58–66.

Perrins, W. T., McKenzie, D. R., and McPhedran, R. C., 1979, Transport properties of regular arrays of cylinders, *Proc. R. Soc. Lond.* **A369,** 207–225.

Rayleigh, Lord, 1892, On the influence of obstacles arranged in rectangular order upon the property of a medium, *Phil. Mag.* **34,** 481–502.

Rifai, M. N. E., Kaufman, W. J., and Todd, D. N., 1956, Dispersion phenomena in laminar flow through porous media, Sanitary Engng. Res. Lab. Rep. No 3, IER Series 90, Univ. of California, Berkeley.

Saffman, P. G., 1959, A theory of dispersion in a porous medium, *J. Fluid. Mech.* **6,** 321–349.

Saffman, P. G., 1960, Dispersion due to molecular diffusion and macroscopic mixing in flow through a network of capillaries, *J. Fluid Mech.* **7,** 194–208.

Shapiro, M. and Brenner, H., 1988, Dispersion of a chemically reactive solute in a spatially periodic model of a porous medium, *Chem. Engng. Sci.* **43,** 551–571.

Simon, R. and Kelsey, F. J., 1971, The use of capillary tube networks in reservoir performance studies: I. Equal-viscosity miscible displacements, *Soc. Petr. Engrs.* **11,** 99–112.

Simon, R. And Kelsey, F. J., 1972, The use of capillary tube networks in reservoir performance studies: I. Equal-viscosity miscible displacements, *Soc. Petr. Engrs.* **12,** 345–361.

Simpson, E. S., 1969, Velocity and the longitudinal dispersion coefficient in flow through porous media, In R. J. M. Wiest (eds), *Flow Thorough Porous Media*, Academic Press, New York, pp. 201–214.

Slichter, C. S., 1905, Field measurement of the amount of underground waters, Water Supply Paper No. 14r, U.S. Geological Survey.

Tardos, G. I. and Gutfinger, C., 1979, Predictions of high Péclet number mass transfer in granular beds using the constricted tube model, *AIChE J.* **25,** 1073–1077.

Taylor, G. I., 1953, Dispersion of soluble matter in solvent flowing slowly through a tube, *Proc. R. Soc. Lond.* **A219,** 186–203.

Taylor, G. I., 1954, The dispersion of matter in turbulent flow through a pipe, *Proc. R. Soc. Lond.* **A223,** 446–468.

Wooding, R. A., 1960, Instability of a viscous fluid of variable density in a vertical Hele–Shaw cell, *J. Fluid Mech.* **7,** 501–515.